CrossMark

Mechanical Properties of Lightweight Porous Magnesium Processed Through Powder Metallurgy

NING ZOU[1] and QIZHEN LI[1,2]

1.—School of Mechanical and Materials Engineering, Washington State University, Pullman, WA 99164, USA. 2.—e-mail: qizhen.li@wsu.edu

Porous magnesium (Mg) samples with various overall porosities ($28.4 \pm 1.8\%$, $35.5 \pm 2.5\%$, $45.4 \pm 1.9\%$, and $62.4 \pm 2.2\%$) were processed through powder metallurgy and characterized to study their mechanical properties. Different porosities were obtained by utilizing different mass fractions of space holder camphene. Camphene was removed by sublimation before sintering and contributed to processing porous Mg with high purity and small average pore size. The average pore size increased from 5.2 μm to 15.1 μm with increase of the porosity from $28.4 \pm 1.8\%$ to $62.4 \pm 2.2\%$. Compressive strain–stress data showed that the strain hardening rate, yield strength, and ultimate compressive strength decreased with increase of the porosity. The theoretical yield strength of porous Mg obtained using the Gibson–Ashby model agreed with experimental data.

INTRODUCTION

Porous Mg is promising for use as a lightweight material and for biodegradable implants due to its good biomedical and mechanical properties.[1–12] The introduction of pores into Mg decreases the density further, creates space for liquid and gas permeability and tissue ingrowth, and increases the impact energy absorption ability.[1–12] Several different methods have been developed to fabricate porous Mg recently, such as powder metallurgy with addition of space holders,[1–10] unidirectional solidification of molten Mg under pressurized gas atmosphere (H_2, Ar),[13,14] melt Mg infiltration,[15,16] jointing of Mg bars,[17] laser perforation,[18] and negative salt-pattern molding process.[19–23]

Camphene has been used as a space holder to produce porous materials such as porous titanium,[24] hydroxyapatite,[25] and zirconium dioxide.[26] Camphene has high vapor pressure and can be sublimated at room temperature.[24–26] Camphene has several advantages over other reported space holders used to fabricate porous Mg through powder metallurgy, such as carbamide,[1–4] ammonium bicarbonate,[5] and poly(methyl methacrylate) (PMMA).[6] Firstly, it is environmentally friendly. Also, camphene sublimates out before sintering, while other space holders are removed by decomposition during sintering. Moreover, sublimated camphene can be reused as a space holder, representing an important economic benefit for industrial fabrication of large amounts of porous material. Secondly, it can result in high-purity products. After sublimation of camphene, the possibility of importing impurities is reduced. Thirdly, other reported space holders have certain particle size, while mixing with liquid camphene does not introduce a size limit, enabling smaller average pore size.

However, to the best knowledge of the authors, camphene had not yet been used for fabricating porous Mg. In the work presented herein, camphene was used as space holder to fabricate porous Mg through powder metallurgy. The microstructure and mechanical properties of the fabricated porous Mg were investigated.

EXPERIMENTAL PROCEDURES

Mg powder (Alfa Aesar, $\sim$ 99.8% purity, $\sim$ 325 mesh) and camphene (95% purity, $C_{10}H_{16}$, Sigma-Aldrich, melting point 48–52°C, density 0.850 g cm^{-3}) were used as starting materials. The Mg powder and its size distribution are shown in Fig. 1a and b, with average size of 45.3 μm.

Porous Mg was fabricated by following four steps: mixing, compacting, sublimating, and sintering. Mg powder and camphene were mixed in a beaker at 60°C for 5 min, with this duration chosen for better mixing
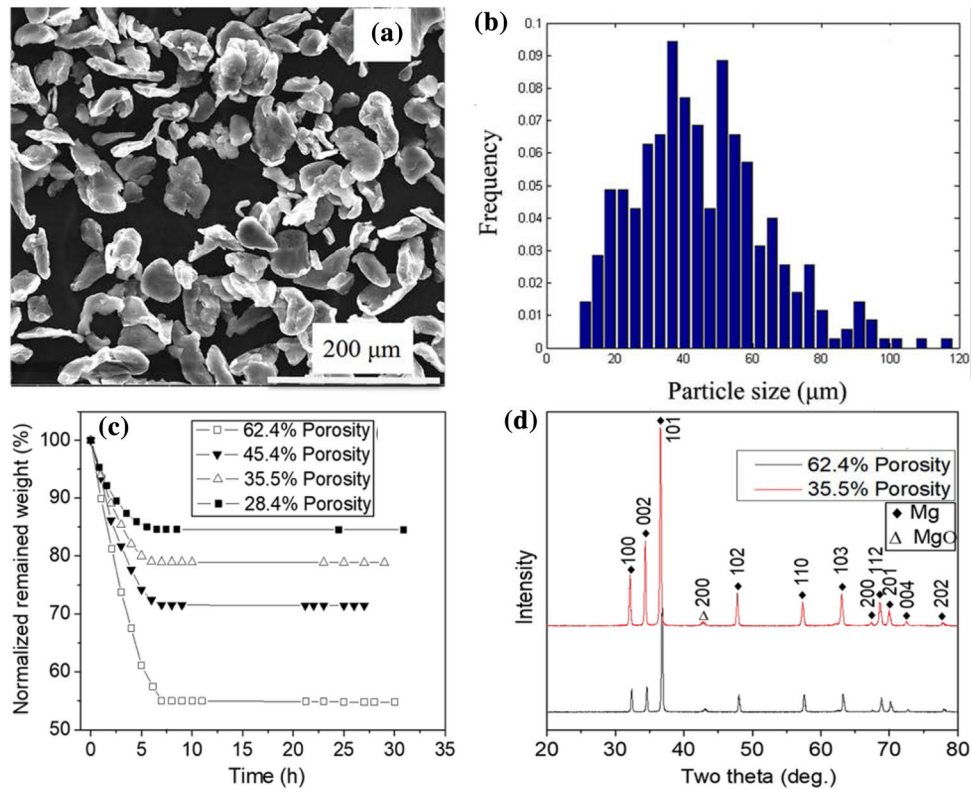
(Published online February 15, 2018)

Fig. 1. (a) SEM micrograph of pure Mg particles used to fabricate porous Mg. (b) Size distribution of Mg particles. (c) Normalized remaining weight versus sublimation time for different camphene–Mg green compacts. (d) Indexed x-ray diffraction pattern of 62.4% and 35.5% porous Mg; peaks for Mg and MgO are labeled by diamond and triangle, respectively.

and less sublimation of camphene, as camphene sublimated quickly at high temperature. The camphene–Mg mixtures were solidified at 20–25°C. Then, the solidified mixture was pressed in a pellet mold to form green compacts using a uniaxial hydraulic press at ~ 500 MPa for 5 min. Next, the green compacts were kept under medium vacuum at room temperature for 1 week to sublimate camphene completely. Medium vacuum pressure was applied so as not to damage the samples during sublimation. Lastly, the green compacts were sintered through a two-step sintering process under inert gas protection. The first sintering step at 250°C for 2 h was applied to remove possible remaining camphene. The second sintering step at 630°C for 6 h was applied to sinter the compacts into porous Mg. Samples with different mass fractions of camphene formed porous Mg with porosity of $62.4 \pm 2.2\%$, $45.4 \pm 1.9\%$, $35.5 \pm 2.5\%$, and $28.4 \pm 1.8\%$, denoted hereinafter using their average porosity.

Optical microscopy (OM) and scanning electron microscopy (FEI SEM Quanta 200F, Field Emission Instruments) were used to characterize the microstructure of the porous Mg samples. The samples were ground using sandpapers with different grits and polished using 1-μm alumina suspension. The sintered samples were analyzed by x-ray diffraction (XRD, Rigaku Miniflex 600) to verify that they were pure Mg. The constituent phases were

detected by XRD using Cu K$_\alpha$ radiation at a scanning rate of 4 min^{-1}. Compression tests were carried out on specimens with height of about 6 mm, length of about 5 mm, and width of about 5 mm at room temperature with a strain rate of $\sim 10^{-3}$/s. The compressive loading direction parallel to the pressing direction is designated as normal orientation, while the compressive loading direction perpendicular to the pressing direction is designated as in-plane orientation. The stress and strain were obtained from load–displacement data. For each type of porous Mg, four repeats were performed.

The overall porosity P was computed using the mass and dimensions of the sample as follows:

$$P = 1 - (m_s/V_s)/\rho_{Mg}, \qquad (1)$$

where ρ_{Mg} is the theoretical density of Mg (1.738 g cm^{-3}) and m_s/V_s is the density of the sample calculated using its mass (m_s) and volume (V_s). The average pore size and average distance between pores were measured by line interception method based on the OM/SEM microstructure.

RESULTS

Sublimation of Camphene

Figure 1c shows the sublimation rates of camphene in camphene–Mg green compacts used to fabricate porous Mg with porosity of 62.4%, 45.4%,

35.5%, and 28.4%. The samples after sublimation were Mg powder with fragile structure. The higher the fraction of camphene in the camphene–Mg mixture, the higher the sublimation rate, as shown in Fig. 1c. A possible reason is that higher fraction of camphene in the camphene–Mg mixture would result in higher porosity after initial camphene sublimation, contributing to further sublimation of camphene. After sublimation for about 7.5 h, the curves became nearly horizontal; i.e., most camphene had sublimated out. Based on these sublimation curves, sublimation for 24 h was used in further experiments to remove camphene before sintering.

Microstructure

Figure 1d shows the XRD patterns of 62.4% and 35.5% porous Mg, revealing high-purity porous Mg with a small amount of MgO remaining as second phase, characterized by the (200) peak at 42.8°. Figure 2 shows the microstructure of fabricated Mg with different porosities of 62.4%, 45.4%, 35.5%, and 28.4%. In these micrographs, dark regions (indicated by arrows) are pores, while bright/yellow regions are Mg. The pores for each type of sample have different sizes.

Mechanical Properties

The compressive engineering stress–strain curves are shown in Fig. 3a. For porous Mg with porosity of 62.4%, 45.4%, and 35.5%, the sample started to deform elastically, then yielded and reached a plateau region before ending with a densification region under applied loading. However, the 28.4% porous Mg specimen exhibited an elastic deformation region followed by a very long strain hardening region, suggesting that strain occurred mainly via bulk deformation. This stress–strain behavior is similar to that of porous Mg fabricated by the mechanical perforation method,[18] replication process using NaCl as space holder,[22] and titanium wire space holder method.[15]

The Young's modulus, strain hardening rate, yield strength, and ultimate compressive strength (UCS) values are shown in Fig. 3c–e. The Young's modulus changed from 465.4 ± 293.7 MPa to 16.2 ± 6.2 MPa along normal orientation and from 1041.2 ± 424.3 MPa to 33.6 ± 1.2 MPa along in-plane orientation, with increase of the porosity from 28.4% to 62.4%. The strain hardening rate decreased from 162.7 ± 62.1 MPa to 4.8 ± 2.3 MPa along normal orientation and from 212.0 ± 36.8 MPa to 7.2 ± 1.9 MPa along in-plane orientation, with increase of the porosity from 28.4% to 62.4%. Both the yield strength and UCS decreased with increasing porosity, in agreement with results reported by other researchers.[1,10,17] Specifically, for our fabricated porous Mg, with increase of the porosity from 28.4% to 62.4%, the yield strength decreased from 16.2 ± 4.1 MPa to 0.7 ± 0.2 MPa along normal orientation and from 17.0 ± 3.4 MPa to 0.596 ± 0.065 MPa along in-
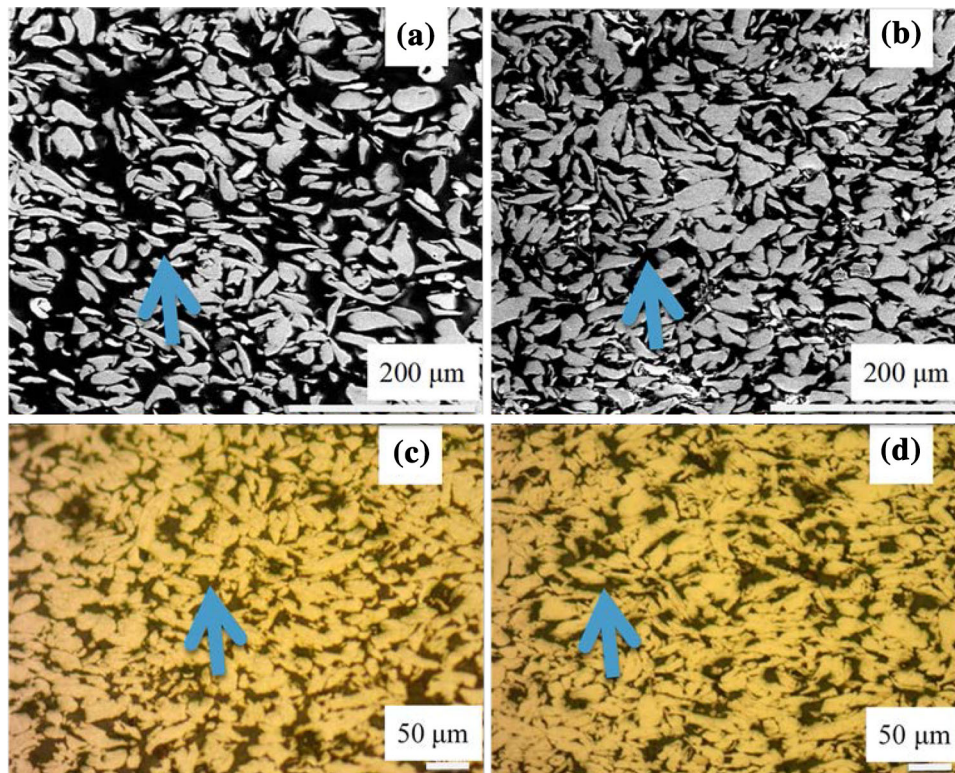

Fig. 2. Microstructure of fabricated porous Mg with (a) 62.4, (b) 45.4, (c) 35.5, and (d) 28.4% porosity.
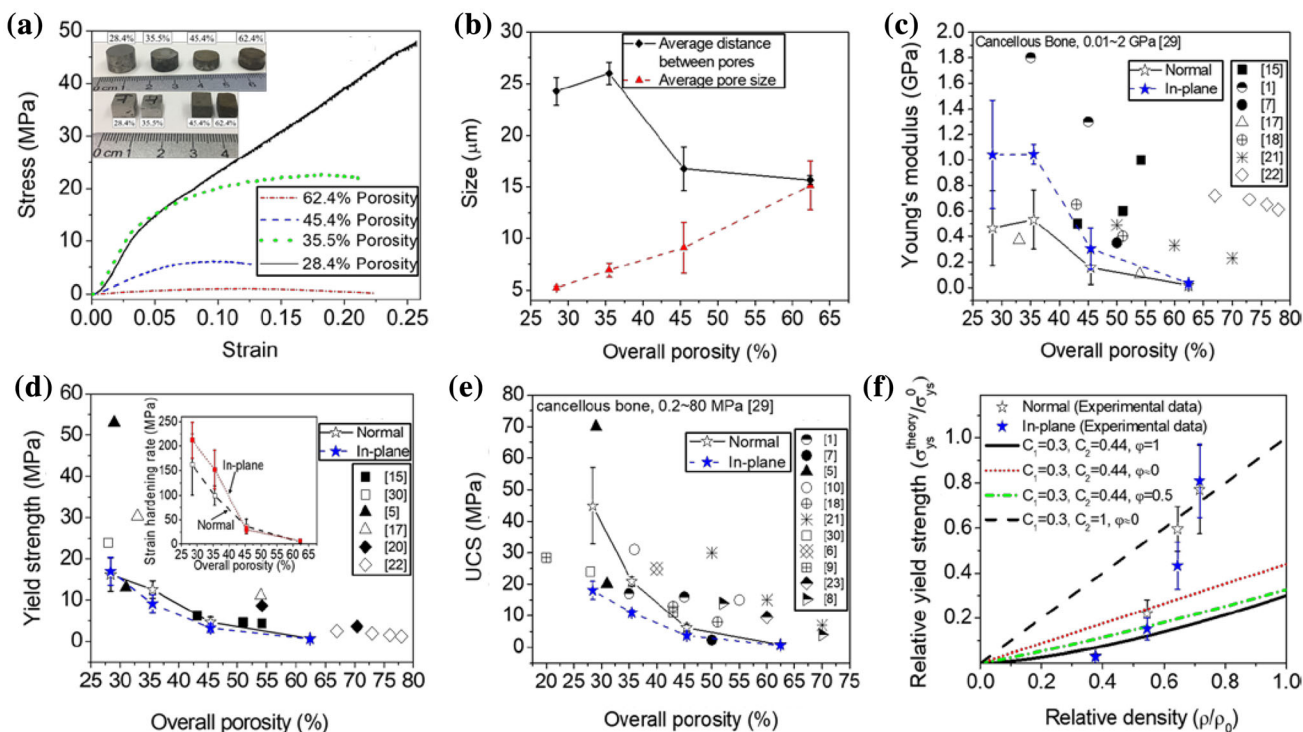
Fig. 3. (a) Engineering strain–stress curves and macrophotography of samples. (b) Average pore size and average distance between pores for porous Mg with various overall porosities. Summary of mechanical properties of experimental data (normal and in-plane orientations), cancellous bone, and recently reported porous Mg samples using different space holders and processing methods: (c) Young's modulus, (d) yield strength, and (e) ultimate compressive strength. (f) Relative yield strength versus relative density of experimental data (normal and in-plane orientations) and different models in Eq. 2.

plane orientation, while the UCS decreased from 44.9 ± 12.1 MPa to 0.8 ± 0.3 MPa along normal orientation and from 18.0 ± 2.9 MPa to 0.624 ± 0.057 MPa along in-plane orientation. The average values of yield strength showed slight difference between normal and in-plane orientation, in agreement with our previous findings on porous Mg reinforced by carbon tube with porosity of 30% and 40%.[2] The average value of Young's modulus along normal orientation was lower than for in-plane orientation, while the average value of UCS along normal orientation was higher than for in-plane orientation.

DISCUSSION

Microstructure

The (200) peak in Fig. 1d shows that our samples contained very little MgO. MgO has also been found in other sintered porous Mg obtained by powder metallurgical method using space holders.[2,5,6,10] For quantitative phase analysis, the volume fraction ratio between MgO and Mg can be estimated from the $I_{(200)\text{-MgO}}/I_{(101)\text{-Mg}}$ ratio.[27] The $I_{(200)\text{-MgO}}/I_{(101)\text{-Mg}}$ ratio for 62.4% and 35.5% porous Mg was 3.3% and 2.5%, respectively. There is no gas waste when fabricating porous Mg using camphene as space holder, as camphene sublimates before sintering. Meanwhile, other space holders are removed during

sintering by decomposition into small compounds such as CO_2,[1] NH_3,[28] or C_2H_4 and CH_3COOH,[6] and impurities may be introduced.

The average pore size increased almost linearly with increase of the porosity, as shown in Fig. 3b. This kind of relationship was also reported in previous research.[2] With increase of the porosity from 28.4% to 62.4%, the average pore size increased from 5.2 μm to 15.1 μm. Particulate space holders, such as carbamide, ammonium bicarbonate, and PMMA, were reported to result in smallest average pore size of 73 μm, as presented in Table I. Camphene contributes to processing porous Mg with smaller average pore size, compared with other particle space holders. Moreover, the average distance between pores decreased with increase of the porosity, except for the 28.4% porous Mg, as shown in Fig. 3c. For the samples with porosity of 62.4% and 45.4%, the average distance between pores was similar, suggesting that this distance is determined by the size of the Mg cell walls, as shown in Fig. 2a and b. The 28.4% and 35.5% porous Mg samples showed longer distance values compared with the 45.4% and 62.4% porous Mg samples. For the samples with porosity of 35.5% and 28.4%, the average distance between pores was determined by both the number and size of pores. Therefore, the average distance between pores did not decrease with increasing porosity.

Table I. Summary of mechanical properties of cancellous bone and porous Mg obtained using different space holders and processing methods (PM represents powder metallurgy)

Material	Processing method	Porosity (%)	Average pore size (μm)	Young's modulus (GPa)	Yield strength (MPa)	UCS (MPa)	References
Cancellous bone	–	–	–	0.01–2	–	0.2–80	Ref. [29]
Porous Mg	PM, carbamide	35	250	1.8	–	17	Ref. [1]
Porous Mg	PM, carbamide	45	73	1.3	–	16	Ref. [1]
Porous Mg	PM, carbamide	50	200–500	0.35	–	2.33	Ref. [7]
Porous Mg	PM, carbamide	52–70	~1250	–	–	4–14	Ref. [8]
Porous Mg	PM, carbamide	36–55	200–400	–	–	15–31	Ref. [10]
Porous Mg	PM, carbamide	20–43	–	–	–	11–28.5	Ref. [9]
Porous Mg	PM, ammonium bicarbonate	29–31	250–500	–	13–53	20–70	Ref. [5]
Porous Mg	PM, PMMA	40	~100	–	–	25	Ref. [6]
Porous Mg	Melt infiltration, Ti wires	43.20	–	0.5	6.2	–	Ref. [15]
Porous Mg	Melt infiltration, Ti wires	51	–	0.6	4.6	–	Ref. [15]
Porous Mg	Melt infiltration, Ti wires	54.20	–	1	4.3	–	Ref. [15]
Porous Mg	Melt infiltration, Ti wires	20–65	270	–	32–2.9	–	Ref. [16]
Porous Mg	Melt infiltration, Ti wires	22–65	400	–	33–3.3	–	Ref. [16]
Porous Mg	Melt solidified	28 ± 1.3	170 ± 19	–	23.9 ± 4.9	24	Ref. [30]
Porous Mg	Mg fiber joint	33	–	0.37	30.3	–	Ref. [17]
Porous Mg	Mg fiber joint	54	–	0.1	11.1	–	Ref. [17]
Porous Mg	Laser perforation	43–51	–	0.4–0.65	–	8–13	Ref. [18]
Porous Mg	Dissolve, salt (NaCl)	54.4–70.4	–	–	3.57–8.65	–	Ref. [20]
Porous Mg	Dissolve, salt (NaCl)	50	–	0.49	–	30	Ref. [21]
Porous Mg	Dissolve, salt (NaCl)	60	–	0.33	–	15	Ref. [21]
Porous Mg	Dissolve, salt (NaCl)	70	–	0.23	–	7	Ref. [21]
Porous Mg	Dissolve, salt (NaCl)	78	–	0.61	1.2	–	Ref. [22]
Porous Mg	Dissolve, salt (NaCl)	76	–	0.65	1.5	–	Ref. [22]
Porous Mg	Dissolve, salt (NaCl)	73	–	0.69	1.9	–	Ref. [22]
Porous Mg	Dissolve, salt (NaCl)	67	–	0.72	2.5	–	Ref. [22]
Porous Mg	Spark plasma, salt (NaCl)	60	240	–	–	9.5	Ref. [23]

Mechanical Properties

Table I summarizes the mechanical properties of porous Mg materials reported to date using several different processing methods, including powder metallurgy, melt Mg infiltration, Mg fiber joint, laser perforation, and dissolved space holder (salt). The space holders used include carbamide, ammonium bicarbonate, Ti wires, and salt (NaCl). The reason for some missing information in Table I is that they were not reported. The mechanical properties in Table I and our data plotted in Fig. 3c–e confirm that our results are comparable to those of other research at similar porosities, regardless of processing method and pore size. We also conclude that samples with smaller average pore size had higher UCS when using the same processing method; For example, the UCS of porous Mg reported by Wen et al.,[1] who used powder metallurgy with urea as space holder, was 17 MPa (porosity 35%, average pore size 250 μm), while our result is 20.9 ± 1.5 MPa (porosity 35.5%, average pore size 7.0 μm). This result indicates an increase of the mechanical properties on decreasing the average pore size. Moreover, note also that the UCS of porous Mg in the present work is close to that of natural bone (0.2–80 MPa),[29] indicating that our fabricated porous Mg has potential for use in bone implants.

Gibson–Ashby Model

The following Gibson–Ashby model[31] was applied to predict the theoretical yield strength of porous materials:

$$\frac{\sigma_{ys}^{theory}}{\sigma_{ys}^{0}} = C_1\left(\varphi\frac{\rho}{\rho_0}\right)^{\frac{3}{2}} + C_2(1-\varphi)\left(\frac{\rho}{\rho_0}\right), \qquad (2)$$

where σ_{ys}^{0} is the yield strength of the dense material composing the studied porous material, C_1 and C_2 are constants (generally 0.3 and 0.44, respectively, and varying for different types of porous material), φ is the volume fraction of the solid in the pore edges for close-cell foams (where $\varphi = 1$ refers to the case that all pores are open and $\varphi \approx 0$ for closed-cell foams with negligible cell edges), ρ and ρ_0 are the density of the porous and dense materials, respectively (with ρ/ρ_0 being the relative density of the porous materials), and $\sigma_{ys}^{theory}/\sigma_{ys}^{0}$ is the relative yield strength. According to Ref. [32], the ρ_0 and σ_{ys}^{0} values for pure dense Mg are 1.738 g cm^{-3} and 21 MPa, respectively.

In this study, we chose the parameter sets $(C_1 = 0.3,\ C_2 = 0.44,\ \varphi = 1)$, $(C_1 = 0.3,\ C_2 = 0.44,\ \varphi = 0.5)$, $(C_1 = 0.3,\ C_2 = 0.44,\ \varphi \approx 0)$, and $(C_1 = 0.3, C_2 = 1,[16]\ \varphi \approx 0)$ in Eq. 2. The corresponding yield strength predictions are plotted in Fig. 3f. $\varphi = 1$, 0.5, and 0 represent different fractions of solid in the pore edges. The experimental data for the 62.4% porous Mg ($\rho/\rho_0 = 0.376$) sample are close to the model with $C_1 = 0.3$, $C_2 = 0.44$, $\varphi = 1$. The experimental data for the 35.5% porous Mg ($\rho/\rho_0 = 0.645$) and 28.4% porous Mg ($\rho/\rho_0 = 0.716$) samples match the model with $C_1 = 0.3$, $C_2 = 1$, $\varphi \approx 0$. The experimental data for the 45.4% porous Mg ($\rho/\rho_0 = 0.546$) sample lie between the model with $C_1 = 0.3$, $C_2 = 0.44$, $\varphi = 1$ and the model with $C_1 = 0.3$, $C_2 = 1$, $\varphi \approx 0$.

CONCLUSION

We investigated the microstructure and mechanical properties of porous Mg with various overall porosities (28.4%, 35.5%, 45.4%, and 62.4%) fabricated by powder metallurgy using camphene as space holder. Camphene was removed by sublimation before sintering, and the fabricated porous Mg had high purity with only small amounts of MgO. Camphene contributed to processing porous Mg with smaller average pore size, compared with particulate space holders. Smaller average pore size resulted in higher UCS when using the same processing method. With increasing porosity from 28.4% to 62.4%, the average pore size increased from 5.2 μm to 15.1 μm. The strain hardening rate, yield strength, and UCS decreased along both normal and in-plane orientations. The average distance between pores and the Young's modulus along normal and in-plane orientations first increased and then decreased with increasing porosity. Strength predictions based on the Gibson–Ashby model matched our experimental data.

ACKNOWLEDGEMENT

REFERENCES

1. C.E. Wen, Y. Yamada, K. Shimojima, Y. Chino, H. Hosokawa, and M. Mabuchi, *Mater. Lett.* 58, 357 (2004).
2. N. Zou and Q. Li, *J. Mater. Sci.* 51, 5232 (2016).
3. H. Cay, H. Xu, and Q. Li, *Mater. Sci. Eng., A* 574, 137 (2013).
4. Q. Li, *Mater. Des.* 89, 978 (2016).
5. J. Capek and D. Vojtech, *Mater. Sci. Eng., C* 35, 21 (2014).
6. Y. Bi, Y. Zheng, and Y. Li, *Mater. Lett.* 161, 583 (2015).
7. C. Wen, M. Mabuchi, Y. Yamada, K. Shimojima, Y. Chino, and T. Asahina, *Scr. Mater.* 45, 1147 (2001).
8. G.L. Hao, F.S. Han, and W.D. Li, *J. Porous Mater.* 16, 251 (2009).
9. J. Shen, Y. Feng, S.-L. Wang, Y. Xu, and X.-B. Zhang, *Met. Funct. Mater.* 3, 003 (2006).
10. H. Zhuang, Y. Han, and A. Feng, *Mater. Sci. Eng., C* 28, 1462 (2008).
11. H. Xu, N. Zou, Q. Li, *JOM* 1 (2017).
12. Q. Li, *Mater. Lett.* 133, 83 (2014).
13. L. Yuan, L. Yanxiang, W. Jiang, and Z. Huawei, *Mater. Sci. Eng., A* 402, 47 (2005).
14. Z.-K. Xie, M. Tane, S.-K. Hyun, Y. Okuda, and H. Nakajima, *Mater. Sci. Eng., A* 417, 129 (2006).
15. G. Jiang and G. He, *Mater. Sci. Eng., C* 43, 317 (2014).
16. G. Jiang, Q. Li, C. Wang, J. Dong, and G. He, *J. Mech. Behav. Biomed. Mater.* 64, 139 (2016).
17. X. Zhang, X.W. Li, J.G. Li, and X.D. Sun, *Mater. Sci. Eng., C* 42, 362 (2014).
18. F. Geng, L. Tan, B. Zhang, C. Wu, Y. He, J. Yang, and K. Yang, *J. Mater. Sci. Technol.* 25, 123 (2009).
19. T.L. Nguyen, M.P. Staiger, G.J. Dias, and T.B.F. Woodfield, *Adv. Eng. Mater.* 13, 872 (2011).
20. X. Wang, Z. Li, Y. Huang, K. Wang, X. Wang, and F. Han, *Mater. Des.* 64, 324 (2014).
21. M.-H. Kang, H.-D. Jung, S.-W. Kim, S.-M. Lee, H.-E. Kim, Y. Estrin, and Y.-H. Koh, *Mater. Lett.* 108, 122 (2013).
22. J.O. Osorio-Hernández, M.A. Suarez, R. Goodall, G.A. Lara-Rodriguez, I. Alfonso, and I.A. Figueroa, *Mater. Des.* 64, 136 (2014).
23. M.H. Kang, T.S. Jang, S.W. Kim, H.S. Park, J. Song, H.E. Kim, K.H. Jung, and H.D. Jung, *Mater. Sci. Eng., C* 62, 634 (2016).
24. S.-W. Yook, H.-E. Kim, and Y.-H. Koh, *Mater. Lett.* 63, 1502 (2009).
25. E.-J. Lee, Y.-H. Koh, B.-H. Yoon, H.-E. Kim, and H.-W. Kim, *Mater. Lett.* 61, 2270 (2007).
26. J. Han, C. Hong, X. Zhang, J. Du, and W. Zhang, *J. Eur. Ceram. Soc.* 30, 53 (2010).
27. R. Jenkins, R.L. Snyder, *Introduction to X-ray Powder Diffractometry*, ed. J.D. Winefordner (New York, Wiley, 1996).
28. J. Capek and D. Vojtech, *Mater. Sci. Eng., C* 33, 564 (2013).
29. L.J. Gibson, *J. Biomech.* 18, 317 (1985).
30. X.N. Gu, W.R. Zhou, Y.F. Zheng, Y. Liu, and Y.X. Li, *Mater. Lett.* 64, 1871 (2010).
31. M.F. Ashby, T. Evans, N.A. Fleck, J. Hutchinson, H. Wadley, L. Gibson, *Metal Foams: A Design Guide* (Elsevier, Amsterdam, 2000).
32. M.M. Avedesian and H. Baker, *ASM Specialty Handbook: Magnesium and Magnesium Alloys* (Materials Park: ASM International, 1999).